FFEMS Fatigue & Fracture of Engineering Materials & Structures
ORIGINAL CONTRIBUTION
doi: 10.1111/ffe.12487

Measurement and prediction of CTOD in austenitic stainless steel

W. KHOR[1,2], P. L. MOORE[3], H. G. PISARSKI[3], M. HASLETT[3] and C. J. BROWN[1]

[1]*Brunel University London, Uxbridge UB8 3PH, UK,* [2]*NSIRC, Granta Park CB21 6AL, UK,* [3]*TWI, Granta Park CB21 6AL, UK*

Received Date: 10 March 2016; Accepted Date: 16 May 2016; Published Online: 2016

ABSTRACT Variation of Crack Tip Opening Displacement (CTOD) test values can have a significant effect on the Engineering Critical Assessment of a structure. This paper examines the development of CTOD with increasing load in an austenitic stainless steel. The silicone replication method giving variation of CTOD across the specimen thickness, and Digital Image Correlation (DIC) are compared to each other, and in turn to clip gauge measurements from tests. Results from Finite Element models are also presented. Estimations of CTOD from BS 7448-1, ISO 12135 and ASTM E1820, and a proposed modification from JWES are compared to the experimental data from the crack cast in silicone compound – assumed to be the actual CTOD. The DIC measurement showed consistency with crack replicas, and a formula is given to estimate CTOD using DIC. For high strain hardening austenitic stainless steel, both the JWES and ASTM E1820 estimations provide adequate accuracy for CTOD.

NOMENCLATURE

A_p = plastic area under P versus V_p
a_0 = initial crack length
B = specimen thickness
B_0 = remaining ligament, $W - a_0$
b = position on section as a ratio of $B/2$
E = modulus of elasticity
$\mathcal{J}$ = strain energy around the crack
K = stress intensity factor
K_I = stress intensity factor in mode I loading
m = plane strain function used in JWES
m_{ASTM} = function relating $\mathcal{J}$ to CTOD
n = strain hardening exponent
P = load
r_p = rotational factor for plastic hinge assumption
V_g = clip gauge opening displacement
V_p = plastic component of clip gauge opening displacement
W = specimen width
z = knife edge height
δ = crack tip opening displacement (CTOD)
δ_5 = direct CTOD measurement from two points at the specimen surface 5 mm apart, placed directly at the crack tip
$\delta_{5\ DIC}$ = δ_5 measured using the DIC technique
δ_{SRC} = CTOD measured on the silicone replicas
δ_{FE} = CTOD obtained from the FE model
v = Poisson's ratio
σ_{ys} =0.2% proof strength at test temperature
σ_{uts} = ultimate tensile strength at test temperature
σ_y = flow stress at test temperature, $(\sigma_{ys} + \sigma_{uts})/2$
ε = strain
η = geometrical based calibration function for $\mathcal{J}$

Correspondence: C. J. Brown. E-mail: chris.brown@brunel.ac.uk
This is an open access article under the terms of the Creative Commons Attribution License, which permits use, distribution and reproduction in any medium, provided the original work is properly cited.

INTRODUCTION

Fracture toughness is used in Engineering Critical Assessment (ECA) to assess the fitness-for-service of engineering structures with respect to avoidance of fracture.[1–5] Differences in the values of fracture toughness measurements on the same specimen using different methods could result in a structure being considered safe or not. It is therefore important that the estimation of failure criteria, such as critical flaw size, does not result in over-conservative design, while still ensuring structural integrity.[6]

Crack Tip Opening Displacement (CTOD) is a measure of the physical opening of an original crack tip in a standard fracture toughness test specimen at the point of stable or unstable crack extension. The CTOD concept was proposed by Wells[7] using notched tension bars. In the early days, a 'COD meter' had been used to measure CTOD.[8] It was placed at the bottom of a sawn notch and the opening of the crack could be measured directly. Modern techniques introduce a fatigue pre-crack in fracture toughness specimens to mimic an actual crack. Displacement data are obtained by measuring the displacement of the load or the opening of the crack mouth (CMOD) from which CTOD is inferred.[9,10]

Current standards-based procedures – such as BS 7448-1,[9] ISO 12135[11] and ASTM E1820[10] – specify methods to determine fracture toughness, including determination of the critical CTOD for the material under the application of slowly increasing loading on the specimen. The fracture test procedure and methodology are well established and are similar between standards. A clip gauge is often used to measure the displacement data from the opening of the crack mouth because of its consistency[12] and simplicity. However, despite the similar testing methods, different standards give different CTOD estimation equations.[13] Figure 1a shows an SENB specimen with the clip gauge attached prior to testing, while Fig. 1b shows the same specimen after testing.

BS 7448-1 and ISO 12135 use the same equation for CTOD based on the assumption of the development of a plastic hinge, while ASTM E1820 calculates CTOD based on a different fracture toughness parameter, J.[14–16] J is defined as the path-independent strain energy around the crack.[17] Recently, researchers at the Japanese Welding Engineering Society (JWES) have suggested a modification to include a strain hardening consideration in the calculation used in BS 7448-1.[18]

A potential application for the JWES strain hardening modification can occur when stainless steel is used. Austenitic stainless steel is often used in harsh environments because of its corrosion resistance properties.[19–22] When compared to typical structural and high strength steel, austenitic stainless steel can have significantly higher strain hardening, which is a result of its high ductility. This ductility usually implies better fracture toughness properties, which in turn leads to reduced engineering safety concerns, but it is still important that this design criterion is assessed. Grade 300 austenitic stainless steel typically contains 18% Chromium, 10% Nickel and 1% Manganese with the balance being made up by Iron.[23]

The current study was carried out to examine the validity of the available standard equations when applied to austenitic stainless steel. In a standard Single Edge Notched Bend (SENB) test, the crack width was estimated using standard clip gauges. Silicone casting and Digital Image Correlation (DIC) were used to measure CTOD directly, and a Finite Element (FE) model was used to simulate the experimental results. The CTOD measurements were not limited to low CTOD values.

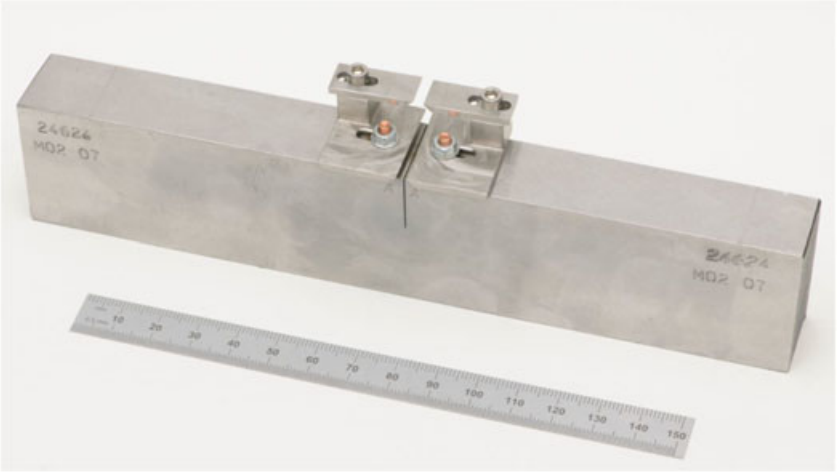

Fig. 1 (a). SENB specimen with double clip gauge attached before loading, (b) SENB specimen after loading without clip gauges.

© 2016 The Authors Fatigue & Fracture of Engineering Materials & Structures Published by John Wiley & Sons Ltd.

MATERIAL AND METHODS

Experiments were carried out using standard SENB testing procedures, in accordance with BS 7448-1 (Fig. 1). SS316 plate was used as the austenitic stainless steel for experimental testing. Mechanical and chemical properties are given in Tables 1 and 2 respectively. Strain hardening, n, was estimated by fitting an offset power law equation to the tensile data obtained from a standard tensile test. Twenty-one-millimetre thick plate was machined to nine standard $B \times 2B$ SENB specimens, where $B = 20$ mm. All SENB specimens are fatigue pre-cracked to a nominal initial crack length of $a_0/W = 0.5$. A full list of all the tests carried out is given in Table 3.

Table 3 Specimen numbering and description

Specimen number	Description	Setup
M03-03	Single point SENB test	
M03-05	Interrupted SENB test with silicone crack replication	
M03-11		Nominally 20 mm × 40 mm B × 2B SENB specimen
M03-12		
M03-13		
M03-14	Single point SENB test with DIC measurement	
M03-15		
M03-16		
M03-17		

Physical crack casting

Physical crack measurement has been a challenge. It is clear from others[24] that a section can be sectioned to measure CTOD – with the consequence that only one measurement per specimen may be made. More recently Tagawa *et al.*[13] and Kawabata *et al.*[18] have used the silicone compound method to replicate the physical crack. However the castings were limited to one per specimen and confined to CTOD ≤ 0.2 mm. A more extensive process is described here.

One of the $B \times 2B$ SENB specimens, labelled M03-05, was used for the physical crack replication test. The crack replication test was similar to a standard test, except that the specimen was held at constant displacement at chosen loads, while a two-part silicone compound (Microset RF-101) was used to make a cast of the crack (Fig. 2a). After the silicone compound had cured (approximately 5 min for each casting), the specimen was further loaded and held at the next chosen load (Fig. 2b), when it was possible to remove the cured crack replica (Fig. 2c), and the casting procedure was then repeated.

Table 1 Tensile properties tested in accordance to BS EN ISO 6892-1:2009 B

Material	SS316
Strain hardening, n[a]	0.53
Plate thickness, mm	21
Yield to tensile ratio, σ_{ys}/σ_{uts}	0.48
0.2% offset proof strength, MPa	285.5
Tensile strength, MPa	595.3
Elongation, %	67.5

[a]Strain hardening measurement is based on curve fitting using offset power law equation.

Image measurements

Image measurements are becoming more viable to measure crack development. The δ_5 method was first devised in the 1980s in Germany.[25] δ_5 is the displacement between two fixed measurement points set initially 5 mm apart on the specimen surface at both sides of the crack tip. For a standard δ_5 test, a special instrument called a δ_5 clip is used to measure the CTOD directly, and the displacement is recorded as the increasing loading is applied. Others adopted the technique and report initial work on thin specimens.[26] More recently Ktari *et al.*[27] have used DIC effectively for crack opening measurement.

DIC measurement was applied on seven different fracture toughness specimens (M03-11 to M03-17), which were tested in a single point SENB setup. A commercial non-contact optical 3D deformation measuring system, GOM-ARAMIS v6.3, was used during these tests to determine δ_5.

By using GOM-ARAMIS, the software is able to recognize the surface structure of the measured object in digital camera images and allocates coordinates to the image pixels. Hence, instead of using δ_5 clips, two stage points with a distance of 5 mm can be defined directly on the recorded images, the displacements of the two points can be obtained from the recorded series of testing images, and δ_5 can be calculated throughout the test. Figure 3 shows the two points recognized on the surface of the specimen for δ_5 measurement, and the displacement of the respective points after the specimen is

Table 2 Chemical composition of SS316 by weigh percentage, measured using electrical discharge method

C	Si	Mn	P	S	Cr	Mo	Ni	Al	As
0.021	0.26	1.76	0.037	0.003	17.4	1.94	10.1	<0.01	<0.01
B	**Co**	**Cu**	**Nb**	**Pb**	**Sn**	**Ti**	**V**	**W**	**Ca**
<0.001	0.19	0.37	<0.01	<0.002	0.01	<0.005	0.06	0.07	<0.001

© 2016 The Authors Fatigue & Fracture of Engineering Materials & Structures Published by John Wiley & Sons Ltd.

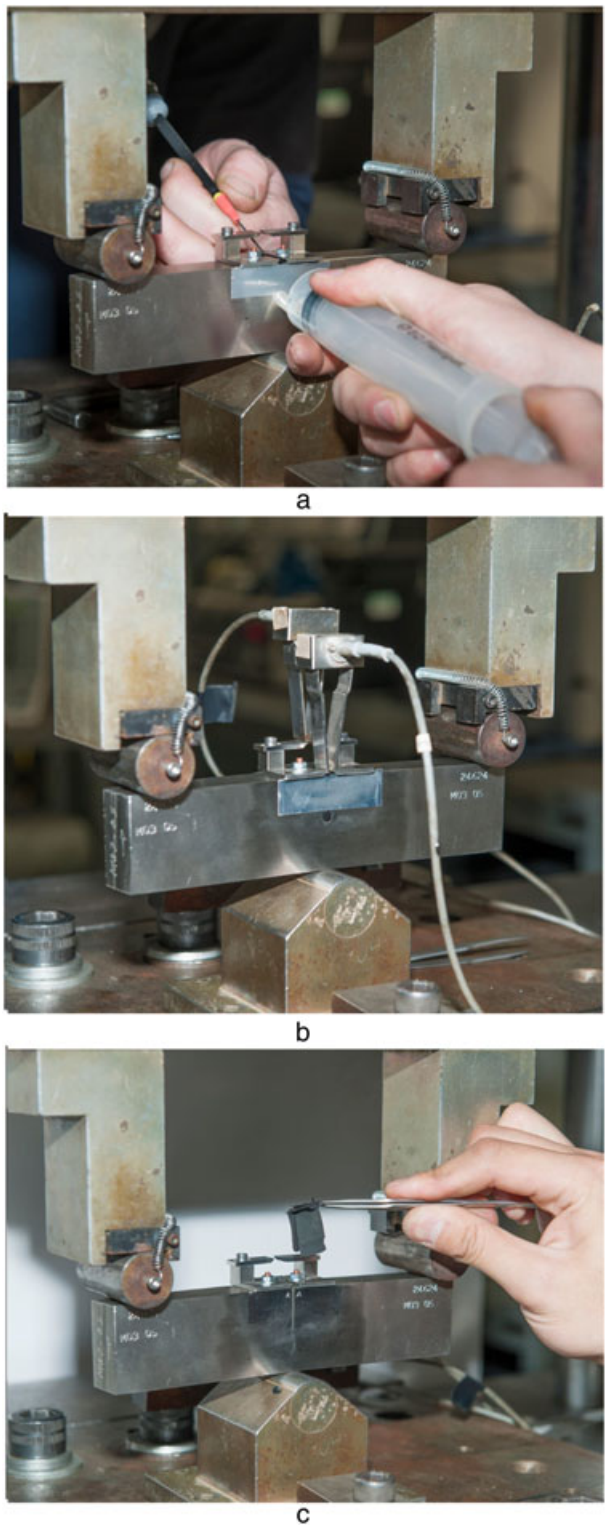

Fig. 2 (a) Crack casting process—filling the crack with silicone compound, (b) crack casting process—specimen further loaded after silicone compound cures, (c) crack casting process—cured crack replica removed from the crack.

loaded. The δ_5 is considered to give an alternative estimation of crack displacement to the CTOD values determined from the standard tests. It provides a direct measurement of CTOD at the surface which may differ from CTOD within the interior of the specimen.

Austenitic stainless steels exhibit high strain hardening and are capable of large plastic deformation. In a three-point-bend test, it was found that the displacement measuring clip gauge often achieved its limit mid-test and required adjustment to continue measurement. DIC, however, measures displacement based on the speckle patterns it recognizes on the surface, which can provide continuous surface displacement measurement.

Finite element models

The FE method has often been applied to investigate fracture toughness estimation equations.[13,18,24,28–30] A Geometrically and Materially Non-linear Analysis (GMNA) FE model was used to predict CTOD in an SENB setup. A fully three-dimensional quarter SENB model was simulated using commercially available software (ABAQUS v6.14) with a blunted crack tip of 0.03 mm radius. The blunted crack tip allows better deformation of the crack tip at larger deformation level. Symmetry was defined on the x–y plane on the side of the specimen facing in the z-direction and the y-z plane on the unbroken ligament facing the x-direction. Figure 4 shows the outline geometry of the SENB specimen investigated and the detail of the mesh adjacent to the crack. Both 8-noded elements (C3D8R) and 20-noded elements (C3D20R) were used to model the SENB specimen. The 20-noded elements gave a better representation of the actual specimen and thus were used in the subsequent sections.

A modulus of elasticity of 200 GPa and Poisson's ratio of 0.3 was used to define the elastic properties, and the experimentally determined true stress–strain properties used for post-elastic material definition are shown in Fig. 5. Displacement in the negative *y*-direction was applied on the upper roller, whereas the lower roller was fixed. A total of 104 736 elements were generated for the model, and a standard convergence test was performed based on varying the element size distributed across the crack tip. CTOD was measured based on opening of the original crack tip.

RESULTS

The CTOD measured on the Silicone Replica Crack (SRC) was considered as representative of the actual physical crack at the particular loading, and used to compare against the other CTOD measurements, finite element predictions and CTOD estimation equations.

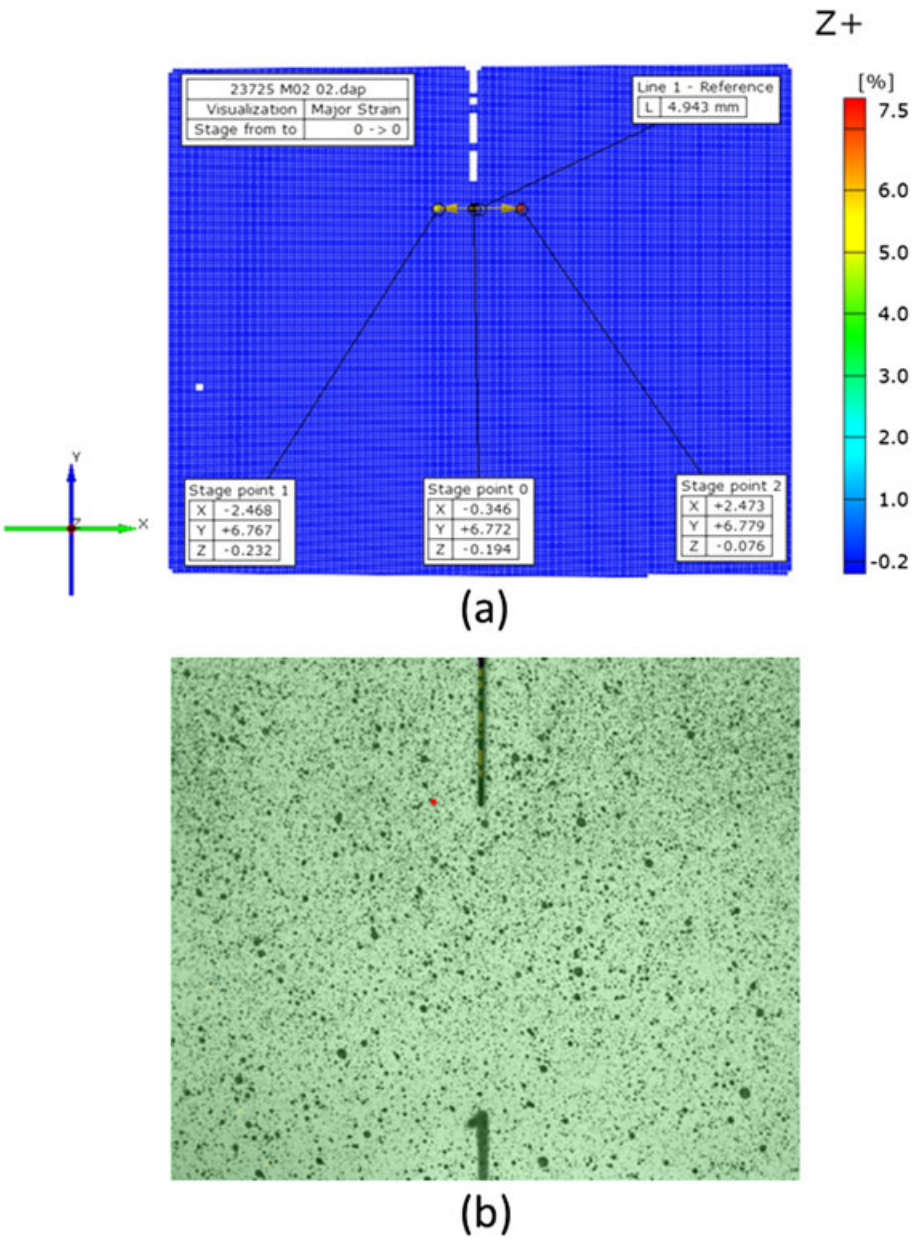

Fig. 3 Determination of (a) δ5 points based on (b) speckle pattern.

In order to compare experimental and FE results, the lower clip gauge opening is converted to CMOD using Equation (1), which is derived from ASTM E1290.[31]

$$CMOD = \frac{Vg}{1 + \frac{z}{0.8a_0 + 0.2W}} \quad (1)$$

Experimental CTOD measurements

Once removed, the silicone replicas were sliced at $b = -0.5$, 0 and 0.5, giving five sections across the replica (Fig. 6). CTOD was then measured on the sliced crack replicas using an optical microscope (Fig. 7). The values of CTOD obtained from the silicone replicas are plotted in Fig. 8 for increasing loads, represented by increasing CMOD.

The specimen was ductile and experienced large deformation in the test. A significant crack tip deformation before tearing, known as the stretch zone, was expected. However the stretch zone width was included in the measurement of original crack length, a_0, because of difficulties in isolating the start and end of the stretch zone width accurately under the microscope. Hence it might be expected that the CTOD measured on the silicone replicas could be fractionally smaller than the actual CTOD.

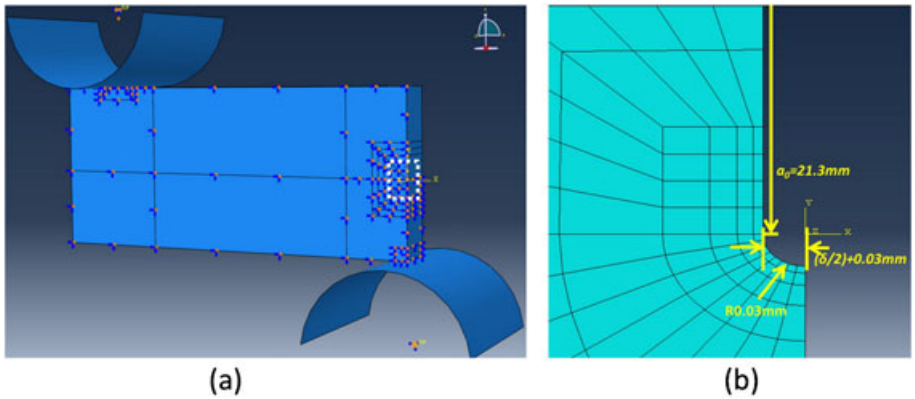

Fig. 4 Quarter SENB model showing boundary conditions, crack shape and mesh near the crack tip.

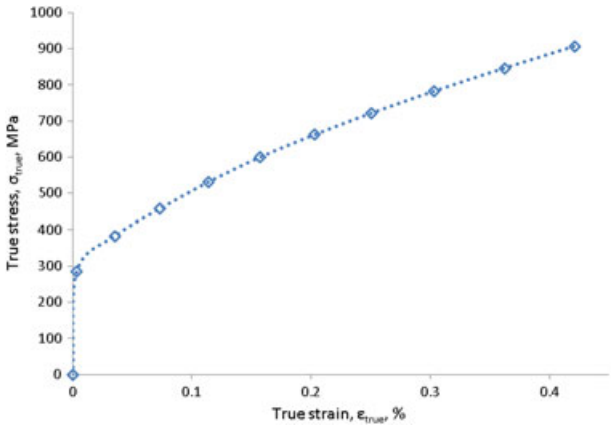

Fig. 5 True stress–strain properties used in the FE model.

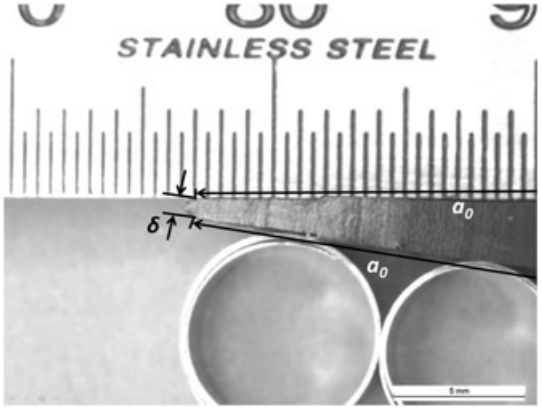

Fig. 7 Definition of CTOD measured on the silicone replica (CMOD = 2.771 mm, b = 0).

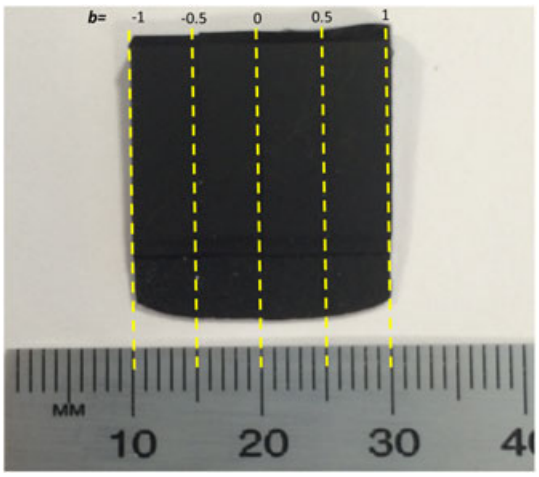

Fig. 6 Silicone crack replica from M03-05, taken at CMOD = 2.031 mm, showing the five equally spaced cross sections for CTOD measurement, described in terms of b, where b = 0 is the middle of the specimen.

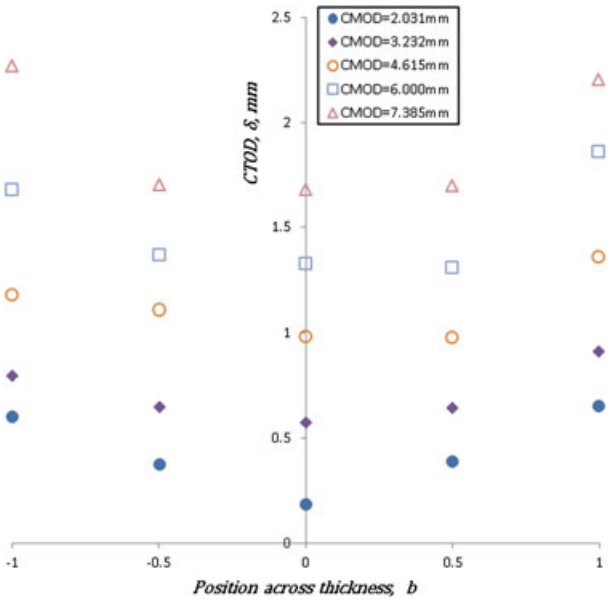

Fig. 8 CTOD at different position across thickness for different CMOD (selected points for clarity).

The load–displacement plot (Fig. 9) for the crack replication test shows load reductions at loads where the crack is replicated by insertion of silicone. This phenomenon is because of load relaxation when the specimen is held at constant displacement.[32] However this phenomenon does not appear to have any significant effect on the overall load–displacement plot and differences between this and a standard test, also shown in Fig. 9 are negligible. The non-linear nature of CMOD with increasing load can be observed.

DIC method for surface measurement

Seven specimens (M03-11 to M03-17) were tested in the SENB configuration. Compiling δ_{5DIC} measurements for each of the seven specimens at loads 10.0 kN, 15.0 kN, 20.0 kN, 25.0 kN and 27.5 kN, and comparing to the clip gauge readings taken at the same load, it was found (Fig. 10) that the $\delta_{5\ DIC}$ measurements were highly correlated to their equivalent clip gauge displacement data ($R^2 = 0.9970$).

Finite element CTOD measurements

The load–displacement relation obtained from the FE model is also shown in Fig. 9. From the FE model, CTOD was determined at three points across the section, $b = 0$ (centre), 0.5 and $b = 1$ (edge). Because of symmetry of the model, these points would also correspond to $b = 0$, -0.5 and -1 in a complete model. Figure 11 shows the relation between CTOD and CMOD, both determined from the FE model. Figure 9 has shown the close agreement between measured and FE modelled CMOD up to a value of about 5 mm; discrepancies that occur after 5 mm are discussed further below.

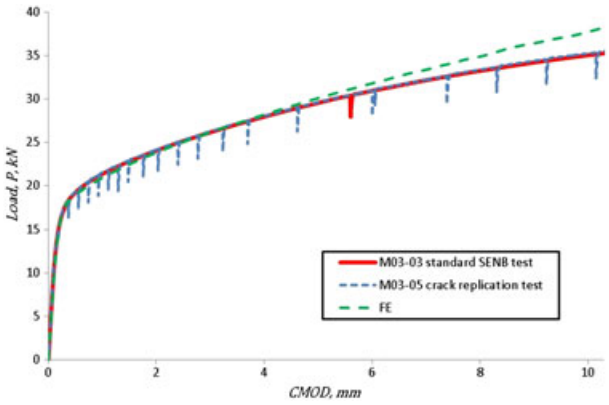

Fig. 9 Load–displacement data obtained from the experiment and FE model.

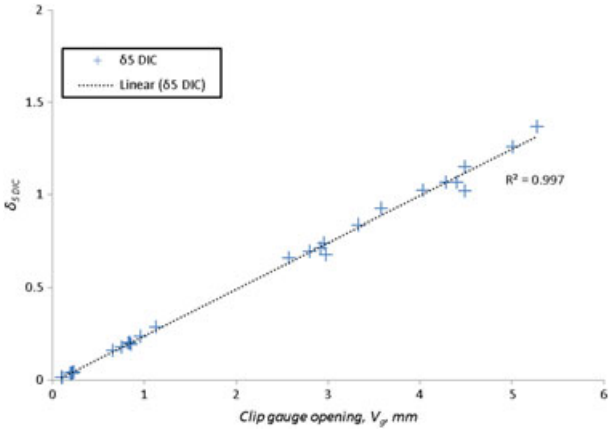

Fig. 10 Clip gauge opening versus δ5 measured on the SS316 SENB specimens tested using DIC.

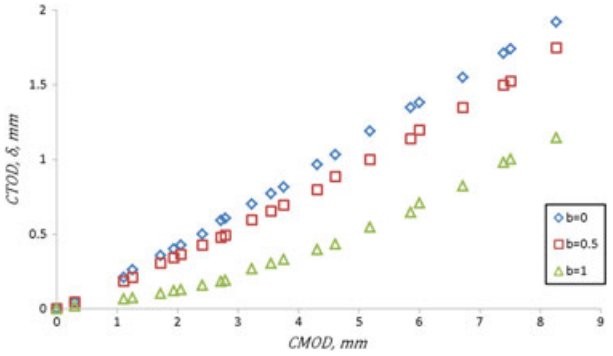

Fig. 11 CMOD versus CTOD at b = 0, 0.5 and 1 obtained from the FE model.

DISCUSSION

The CTOD estimation equations used in the standards (BS 7448-1, ISO 12135 and JWES) were based on research which did not cover material with high strain hardening properties.[33,34] Figure 12 shows CTOD measured from the SRC specimens at the centre ($b = 0$), and the average of the two edge values ($b = \pm 1$), plotted against the value measured using DIC for austenitic stainless steel. The measurements at the surface are both the same estimate of CTOD, and it can be seen that very good agreement is obtained using a linear relation[35] with $R^2 = 0.9974$. DIC measurements might be more conservative than the surface CTOD from SRC at large displacement. This is because the measurements are taken at an offset rather than directly at the crack tip (Fig. 13).[36] However, this not thought to be a problem here.

From Fig. 6 it can be seen that the line defining the crack tip front is curved. The straight crack front FE model (Fig. 11) shows that the CTOD is greater at the

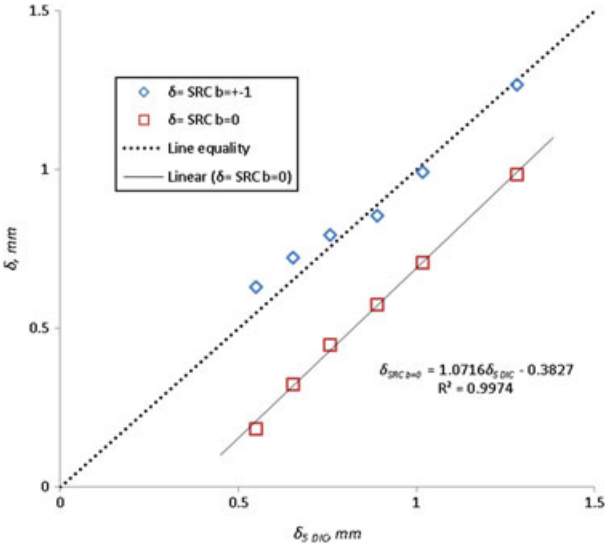

Fig. 12 Comparison between δ5 DIC, δ SRC (b = 0) (plane strain CTOD), and δ SRC (b = ±1) (surface CTOD).

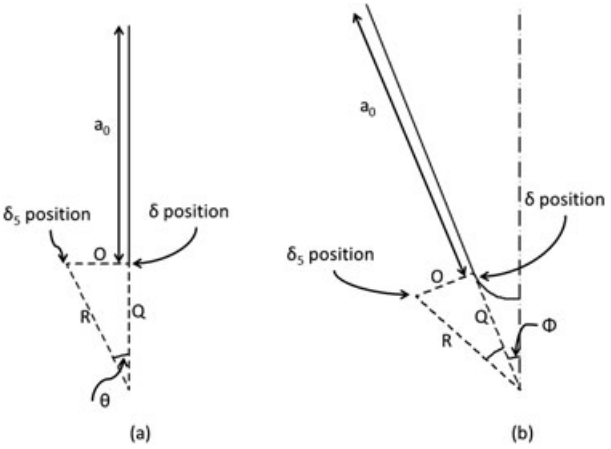

Fig. 13 Geometrical analysis of δ and δ5 on (a) an idealized initial crack and (b) an idealized blunted crack.

crack centre than at the outside surfaces but Fig. 12 shows that the value of δ_{SRC} at the sides is greater than that at the centre. However, from Fig. 14 it can be seen that the geometry and the assumption of a constant point of specimen rotation dictate otherwise, and the curved crack front means a lower value of δ_{SRC} is found at the centre.

A consistent relationship between $\delta_{5\ DIC}$ and $\delta_{SRC\ (b=0)}$ is observed (Fig. 12) for $\delta_{5\ DIC} > 0.5$ mm, indicating a little-changing difference between the crack width at the centre of the specimen and that at the outer edges. CTOD at the centre of the specimen is approximately 0.34 mm lower than at the surface CTOD for the crack front curvature present in this specimen. Equation (2) shows the relation of $\delta_{5\ DIC}$ to $\delta_{SRC\ (b=0)}$.

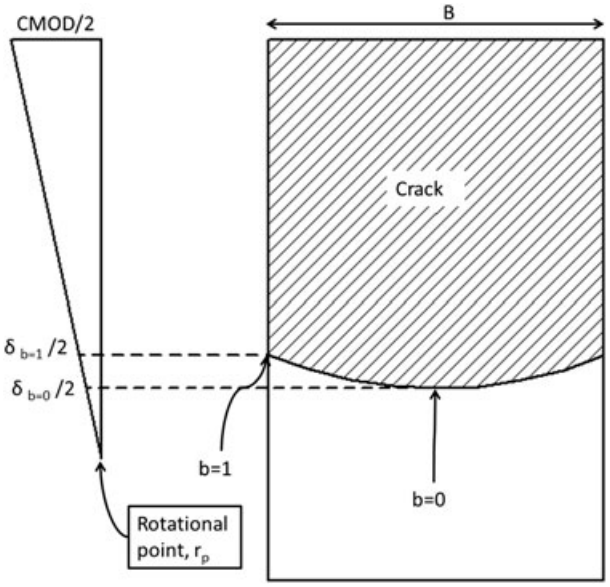

Fig. 14 The effect of curved crack front on the determination of CTOD at the middle and side of the specimen.

$$\delta_{SRC\ (b\ =\ 0)} = 1.0716\delta_{5\ DIC} - 0.3827 \quad (2)$$

The elastic CTOD equations in BS 7448-1, ASTM E1820 and in the JWES equation assume plane strain conditions for the estimation of CTOD. By investigating the strain data across the crack tip obtained from the FE model, it is found that conditions approximating plane strain are achieved across much of the thickness. CTOD at $b = 0$ is considered the 'plane strain' CTOD estimated by the standardized equations; this is discussed further later in the paper.

A straight crack front model was simulated in FE as an idealized test specimen. Pook has provided a useful retrospective[37] of the importance of 3-D effects on the crack front, and in particular, the importance of understanding the consequences of a curved crack front. A linear elastic analysis[38] shows similarities between the FE and stress intensity factor models.

The measured initial crack length of the sides of the specimen tested is shorter than the initial crack length on the middle of the specimen. This phenomenon is a result of the fatigue loading on the specimen, which is used to induce a crack. Figure 11 shows the CTOD obtained at different positions across the crack front, which shows an opposite trend when compared to the CTOD measured from the silicone replicas in Fig. 8. These findings are consistent with Hutchison & Pisarski's[29] FE predictions, where straight crack front models give larger CTOD in the middle of the crack front while a curved crack front model gives larger CTOD in the sides of

the crack. Analysing the effect of crack length using the similar triangles principle used in BS 7448-1, a lower a_0/W ratio (shorter crack length) would result in higher CTOD, as described above for the experimental results.

The CTOD obtained from FE and standardized estimation equations were compared to that measured on the silicone replica (Fig. 15). The FE model and BS 7448-1 overestimate the silicone replica CTOD for all values of CTOD, while ASTM E1820 and JWES overestimate low values of CTOD, but underestimate towards larger CTOD values. Experimentally, stable ductile tearing initiates under large deformation at the crack tip; in the FE model, the crack tip continues deforming under increasing load, as damage mechanisms and crack extension were not accounted for in the model. Figure 15 shows that the FE estimations become close to the SRC measurements at larger CTOD values ($\delta_{SRC\ (b=0)} > 1$ mm). The larger difference observed in lower CTOD values in the FE model is because of the blunted crack tip used which might result in an increase in CTOD when compared to a fatigue pre-cracked notch.[39]

If an underestimation of CTOD up to 15% is considered acceptable, both the JWES equation and ASTM E1820 estimation can be considered to be acceptable predictors of $\delta_{SRC(b=0)}$. Based on CTOD measured in the $\delta_{SRC\ (b=0)} > 1$ mm region, JWES gives a very good estimation of $\delta_{SRC\ (b=0)}$. In the range $\delta_{SRC\ (b=0)} > 0.5$ mm, ASTM E1820 gives a lower value of CTOD, but generally within the 15% limit. The overestimation of the lower values of CTOD is because of the underestimation of the physical CTOD, a result of the inclusion of stretch zone width in the determination of the original crack length, a_0,resulting in the overestimation being more obvious in the lower CTOD region, e.g. $\delta_{SRC\ (b=0)} <$ 0.5 mm. The results suggest that the JWES and ASTM E1820 methods are better alternatives than BS 7448-1 to estimate CTOD in high strain hardening austenitic stainless steels.

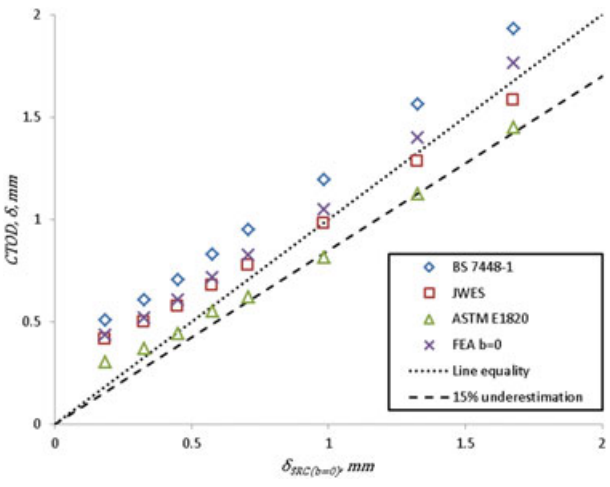

Fig. 15 Comparison of the silicone replica CTOD, δ SRC (b = 0) to FE CTOD, δ FE (b = 0) and standard CTOD estimations.

Based on the results obtained from the silicone replicas and FE, it was found that the Japanese modification to the BS 7448-1 and ISO 12165 equation, and the ASTM E1820 estimation are both recommended for determining CTOD for austenitic stainless steel and high strain hardening materials. The JWES CTOD equation for SENB specimens is given by[18]

$$\delta = K^2 \frac{(1-v^2)}{m\sigma_{ys}E} + f\left(B, \frac{\sigma_{ys}}{\sigma_{uts}}\right) \frac{0.43B_0V_p}{0.43B_0 + a_0 + z}$$

where the correction factors are:

$$m = 4.9 - 3.5\left(\frac{\sigma_{ys}}{\sigma_{uts}}\right)$$

$$f(B) = 0.8 + 0.2exp\{-0.019(B-25)\}$$

$$f\left(\frac{\sigma_{ys}}{\sigma_{uts}}\right) = -1.4\left(\frac{\sigma_{ys}}{\sigma_{uts}}\right)^2 + 2.8\frac{\sigma_{ys}}{\sigma_{uts}} - 0.35.$$

CONCLUSIONS

This paper has shown the measurement of CTOD using silicone replicas. δ_5 DIC measurements have been validated using the silicone replica CTOD data. An FE model has been used to generate predictions of the experimental data.

For austenitic stainless steel and high strain hardening materials, CTOD measured on the silicone replica suggest that JWES give good estimates of CTOD for $\delta_{SRC\ (b=0)} > 1$ mm. The ASTM E1820 estimation is an alternative for measuring $\delta_{SRC\ (b=0)} < 1$ mm.

For high strain hardening materials, direct measurement of δ_5 at the specimen surface using the DIC approach can estimate CTOD for 0.5 mm $< \delta_{5\ DIC}$ using Equation (2). This equation provides a good estimate of CTOD for research applications; however, the use of DIC would not necessarily be practical for commercial test houses.

Acknowledgements

The authors wish to acknowledge the funding and facility provided by TWI and NSIRC for this work. The authors also wish to thank Philip Cossey and Dan Bloom for assistance in the crack replication tests, Mark Tinkler for the setup of the DIC equipment and Prof. Tetsuya Tagawa for the updates and discussion on the silicone crack replication method.

REFERENCES

1 Shen, G., Gianetto, J. A., Bouchard, R., Bowker, J. T., and Tyson, W. R. (2004) Fracture toughness testing of pipeline girth welds. *International Pipeline Conference*. Minister of Natural Resources, Canada, Calgary.

2 Gordon, J. R., Keith, G. and Gordon, N. C. (2013) Defect and strain tolerance of girth welds in high strength pipelines. In: *International Seminar on Welding High Strength Pipeline Steels*, CBMM and TMS: USA, pp. 365–394.

3 Sarzosa, D. F. B., Souza, R. F. and Ruggieri, C. (2015) J–CTOD relations in clamped SE(T) fracture specimens including 3-D stationary and growth analysis. *Eng. Fract. Mech.*, **147**, 331–354.

4 BSI (2014) BS 7910:2013—guide to methods for assessing the acceptability of flaws in metallic structures. BSI.

5 API (2007) API 579—fitness-for-service.

6 Anderson, T. L. and Osage, D. A. (2000) API 579: a comprehensive fitness-for-service guide. *Int. J. Pres. Ves. Pip.*, **77**, 953–963.

7 Wells, A. A. (1969) Crack opening displacements from elastic–plastic analyses of externally notched tension bars. *Eng. Fract. Mech.*, **1**, 399–410.

8 Burdekin, F. M. and Stone, D. E. W. (1966) The crack opening displacement approach to fracture mechanics in yielding materials. *J. Strain. Anal. Eng. Des.*, **1**, 145–153.

9 BSI (1991) BS 7448-1:1991—Fracture mechanics toughness tests — Part 1: Method for determination of KIc, critical CTOD and critical J values of metallic materials. BSI.

10 ASTM (2014) ASTM E1820-13—standard measurement of fracture toughness. ASTM, 1–54.

11 ISO (2002) ISO 12135—02 metallic materials—unified method of test for the determination of quasistatic fracture toughness. ISO.

12 Kirk, M. T. and Dodds, R. H. Jr. (1993) J and CTOD estimation equations for shallow cracks in single edge notch bend specimens. *J. Test. Eval.*, **21**, 228–238.

13 Tagawa, T., Kawabata, T., Sakimoto, T., Kayamoi, Y., Ohata, M., Yamashita, Y., Tamura, E., Yoshinari, H., Aihara, S., Minami, F., Mimura, H. and Hagihara, Y. (2014) Experimental measurements of deformed crack tips in different yield-to-tensile ratio steels. *Eng. Fract. Mech.*, **128**, 157–170.

14 Shih, C. F. (1981) Relationships between the J-integral and the crack opening displacement for stationary and extending cracks. *J. Mech. Phys. Solids*, **29**, 305–326.

15 Kumar, V., German, M. D. and Shih, C. F. (1981) An Engineering Approach for Elastic–Plastic Fracture Analysis. *Electric Power Research Institute Report NP-1931*. General Electric Company, Palo Alto, California.

16 Zhu, X.-K. and Joyce, J. A. (2012) Review of fracture toughness (G, K, J, CTOD, CTOA) testing and standardization. *Eng. Fract. Mech.*, **85**, 1–46.

17 Rice, J. R. (1968) A path independent integral and the approximate analysis of strain concentration by notches and cracks. *J. Appl. Mech.*, **35**, 379–386.

18 Kawabata, T., Tagawa, T., Sakimoto, T., Kayamoi, Y., Ohata, M., Yamashita, Y., Tamura, E., Yoshinari, H., Aihara, S., Minami, F., Mimura, H. and Hagihara, Y. (2016) Proposal for a new CTOD calculation formula. *Eng. Fract. Mech.*, **159**, 16–34.

19 Ebara, R. (2002) Long-term corrosion fatigue behaviour of structural materials. *Fatigue Fract. Eng. Mater. Struct.*, **25**, 855–859.

20 Spindler, M. W. (2004) The multiaxial creep ductility of austenitic stainless steels. *Fatigue Fract. Eng. Mater. Struct.*, **27**, 273–281.

21 Colin, J. and Fatemi, A. (2010) Variable amplitude cyclic deformation and fatigue behaviour of stainless steel 304 L including step, periodic, and random loadings. *Fatigue Fract. Eng. Mater. Struct.*, **33**, 205–220.

22 Rahimi, S. and Marrow, T. J. (2012) Effects of orientation, stress and exposure time on short intergranular stress corrosion crack behaviour in sensitised type 304 austenitic stainless steel. *Fatigue Fract. Eng. Mater. Struct.*, **35**, 359–373.

23 ASTM (2006) ASTM A276-06—standard specification for stainless steel bars and shapes. ASTM, 1–7.

24 Wang, Y.-Y., Reemsnyder, H. S., and Kirk, M. T. (1997) Inference equations for fracture toughness testing: numerical analysis and experimental verification. *ASTM STP 1321*. 469–484.

25 Schwalbe, K.-H. (1995) Introduction of δ_5 as an operational definition of the CTOD and its practical use. *ASTM STP 1256*. 763–778.

26 Ipina, J. E. P. (1997) CTOD with slow stable crack growth: analysis of the elastic component. *Fatigue Fract. Eng. Mater. Struct.*, **20**, 1075–1082.

27 Ktari, A., Baccar, M., Shah, M., Haddar, N., Ayedi, H. F. and Rezai-Aria, F. (2014) A crack propagation criterion based on ΔCTOD measured with 2D-digital image correlation technique. *Fatigue Fract. Eng. Mater. Struct.*, **37**, 682–694.

28 Tagawa, T., Kawabata, T., Sakimoto, T., Kayamoi, Y., Ohata, M., Yamashita, T., Tamura, E., Yoshinari, H., Aihara, S., Minami, F., Mimura, H. and Hagihara, Y. (2014) A new CTOD calculation formula, considering strain-hardening property. *Procedia Mate. Sci.*, **3**, 772–777.

29 Hutchison, E., and Pisarski, H. G. (2013) Effects of crack front curvature on J and CTOD determination in fracture toughness specimens by FEA. *Proceedings of the ASME 2013 32nd International Conference on Ocean, Offshore and Arctic Engineering OMAE 2013*, Nantes, France.

30 Hutchison, E., London, T. (2015) Simulation of stable ductile tearing using re-mesh techniques coupled with nodal release incorporating constraint. *NAFEMS World Congress 2015*, San Diego, USA.

31 ASTM (2008) ASTM E 1290-08—standard test method for crack-tip opening displacement (CTOD) fracture toughness measurement. ASTM, 1–15.

32 Tagawa, T., Haramishi, Y. and Minami, F. (2011) Stress relaxation behavior of low carbon structural steels. *Q. J. Jpn. Weld. Soc.*, **29**, 48–54.

33 Lin, I. H., Anderson, T. L., Derit, R., Dawes, M. G., DeWit, R. and Dawes, M. G. (1982) Displacements and rotational factors in single edge notched bend specimens. *Int. J. Fract.*, **20**, R3–R7.

34 Wu, S.-X. (1983) Plastic rotational factor and J-COD relationship of three point bend specimen. *Eng. Fract. Mech.*, **18**, 83–95.

35 Microsoft (2010) Microsoft Excel.

36 Verstraete, M. A., Denys, R. M., Van Minnebruggen, K., Hertelé, S. and De Waele, W. (2013) Determination of CTOD resistance curves in side-grooved Single-Edge Notched Tensile specimens using full field deformation measurements. *Eng. Fract. Mech.*, **110**, 12–22.

37 Pook, L. P. (2013) A 50-year retrospective review of three-dimensional effects at cracks and sharp notches. *Fatigue Fract. Eng. Mater. Struct.*, **36**, 699–723.

38 Pook, L. P. (2000) Finite element analysis of corner point displacements and stress intensity factors for narrow notches in square sheets and plates. *Fatigue Fract. Eng. Mater. Struct.*, **23**, 979–992.

39 Spink, G. M., Worthington, P. J. and Heald, P. T. (1973) The effect of notch acuity on fracture toughness testing. *Mater. Sci. Eng.*, **11**, 113–117.

© 2016 The Authors Fatigue & Fracture of Engineering Materials & Structures Published by John Wiley & Sons Ltd.